Numerical Studies of Electron Dynamics in Oblique Quasi-Perpendicular Collisionless Shock Waves

P. C. Liewer
V. K. Decyk
J. M. Dawson
B. Lembege

CRPC-TR90081
December, 1990

Center for Research on Parallel Computation
Rice University
P.O. Box 1892
Houston, TX 77251-1892

CRPC-90-11 December 3, 1990

Numerical Studies of Electron Dynamics in Oblique Quasi-Perpendicular Collisionless Shock Waves

P. C. Liewer[1], V. K. Decyk[2], J. M. Dawson[2], and B. Lembège[3]

[1] *Jet Propulsion Laboratory*
California Institute of Technology
Pasadena, California 91125

[2] *Physics Department*
University of California
Los Angeles, California 90022

[3] *CRPE/CNET*

* *This work was supported in part by Caltech President's Fund Grant No. PF-317 and in part by the NSF under Cooperative Agreement No. CCR-8809615. The UCLA research was supported by Caltech President's Fund Grant No. PF-317 and by NSF Contract ATM 89-22133. The government has certain rights in this material.*

Numerical Studies of Electron Dynamics in Oblique Quasi-Perpendicular Collisionless Shock Waves

P. C. Liewer
Jet Propulsion Laboratory, California Institute of Technology

V. K. Decyk and J. M. Dawson
Physics Department, University of California

B. Lembège
CRPE/CNET

Abstract

Linear and nonlinear electron damping of the whistler precursor wave train to low Mach number quasi-perpendicular oblique shocks is studied using a one-dimensional electromagnetic plasma simulation code with particle electrons and ions. In some parameter regimes, electrons are observed to trap along the magnetic field lines in the potential of the whistler precursor wavetrain. This trapping can lead to significant electron heating in front of the shock for low β_e ($\sim$ 10% or less). Use of the 64-processor Caltech/JPL Mark IIIfp hypercube concurrent computer has enabled us to make long runs using realistic mass ratios ($m_i/m_e = 1600$) in the full particle PIC code and thus simulate shock parameter regimes and phenomena not previously studied numerically.

1. Introduction

The problem of shocks in magnetized plasmas is a classic one which has received a great deal of investigation from observations, analytic theory and, more recently, computer modeling. Despite all the effort, many aspects of shocks remain unclear. This is probably not surprising due to the wealth of physical processes which can occur in shocks structures. No one simple all encompassing picture can be expected to cover all such shocks. For example, the shock dissipation can show up as ion heating (perpendicular to the magnetic field or shock front), as electron heating parallel or perpendicular to the field or some combination of both. Such dissipation can come from particle reflection, particle trapping in waves, cyclotron resonance damping or other classical forms of wave damping. It is also possible for the dissipation to come about through instabilities produced by the relative flows of electrons through ions, ions through ions, and through a wide range of parametric instabilities. Conditions both upstream and downstream of a shock will depend on just which of these processes are dominant. Secondary instabilities and nonlinear processes can take place in these regions and these in turn will effect the shock. Exactly which processes will dominate will depend on the details of the conditions in the shock regions (Mach number, shock angle relative to the magnetic field, the electron and ion temperatures and their ratio, the existence of multiple ion species, etc.) Thus the study of shocks in

magnetized plasma will undoubtedly be a subject of interest for some time.

In this paper we study through computer simulation and analysis weak quasi-perpendicular oblique shocks, *e.g.*, shocks with an propagation angle relative the the shock normal in the range $\pi/2 - \sqrt{m_e/m_i} > \theta_{\mathbf{Bn}} > \pi/4$. Such shocks are characterized by a standing whistler wave train preceding the shock [*Tidman and Krall*, 1971]. We show that linear and nonlinear interaction of the electrons with the precursor wave play an important role in these shocks. To study electron kinetic effects in shocks, it is necessary to follow both the ion and electron dynamics, making such codes much more computationally intensive than hybrid (fluid electron-kinetic ion) particle codes. The studies in this paper were carried out on the 64-processor Caltech/JPL Mark IIIfp hypercube concurrent supercomputer which provided the computational power to run this full particle code with realistic mass ratios ($m_i/m_e = 1600$) and extend the earlier studies of electron kinetic effects on shocks [*Lembége and Dawson*, 1987a, 1989] into new parameter regimes.

Weak quasi-perpendicular oblique shocks have been observed in the Earth's bow shock under low β conditions, *e.g.*, Figure 1 from *Mellott and Greenstadt* [1984]. Detailed studies of such shocks by *Mellott and Greenstadt* [1984], using data from the ISEE 1 and 2 dual spacecraft mission, showed that the widths of these low Mach number laminar shocks scaled with the ion inertial length (c/ω_{pi}) as expected theoretically for *dispersive* shocks; no additional dissipation from cross-field streaming instabilities was necessary to explain the measured widths. Studies of the electron and ion heating across such shocks by *Thomsen et al.*[1985] showed greater than adiabatic ($T_\perp \propto B$) heating of both electron and ions across such shocks, indicating some additional dissipative process, but results were inconclusive as to what mechanism caused this heating.

Strong supercritical shocks ($M_A > M_{crit} \sim 4$) are much more common in the earth's bow shock and most numerical work has focused on these. The dominant processes determining the structure of these shocks are ion reflection from the shock potential followed by ion thermalization. Because these processes occur on ion times scales, most numerical simulations of quasi-perpendicular collisionless shocks have used *hybrid* particle ion-fluid electron codes [*Leroy et al.*, 1982; *Leroy et al.*, 1981; *Winske and Leroy*, 1984 and references therein]. By treating the electrons as a magnetized fluid, the computation can be done on the ion, not electron, time scale, drastically reducing computer time requirements. Any electron dissipation is generally included in hybrid codes via an ad hoc anomalous resistivity in Ohm's law, although more sophisticated models have also been used [*Liewer*, 1976]. Hybrid simulations have contributed greatly to the present understanding of collisionless shock waves [*Leroy et al.*, 1982; *Leroy et al.*, 1981; *Winske and Leroy*, 1984].

However, for quasi-perpendicular *oblique* shocks, the electron dynamics may be important because the shock electric fields in the direction of propagation **n** have a component along the magnetic field, $E_\parallel = E_n cos\theta_{\mathbf{Bn}}$, allowing the electrons as well as the ions, to be accelerated by these large electric fields[*e.g.*, *Lembége and Dawson* 1989, 1987a]. In this case, a fluid treatment of electrons may be inadequate. Analysis of ISEE 1 and 2 weak oblique shocks by *Gary and Mellott* [1985] indicated that electron damping of the whistler precursor wave train was important; a self-consistent study of such effects also require a kinetic treatment of electrons.

In our simulations of low Mach number ($M_A \leq 3$) oblique quasi-perpendicular shocks, we have found that electron dynamics play an important role in the shock structure. Specif-

ically, we observe a strong interaction between the upstream electrons and the whistler precursor leading to a damping of the precursor and a heating of the electrons. In some parameter regimes, the electrons are seen to trap along the field lines in the electrostatic potential of the whistler, indicating significant nonlinear damping of the precursor. This can lead to strong electron heating in front of the shock when the parallel phase velocity of the whistler exceeds the electron thermal velocity.

2. Simulation Model

A one-dimensional electromagnetic particle-in-cell code with kinetic electrons and ions was used for these studies. The code uses standard PIC techniques [*Birdsall and Langdon*, 1985] to solve the coupled equation for the particle orbits and the electromagnetic fields as an initial value problem. No ad hoc electron dissipation from cross-field streaming instabilities was included. This code was run on 32 and 64 processor JPL/Caltech Mark IIIfp Hypercube concurrent computers. The parallel electromagnetic code was developed from a parallel electrostatic code implemented using the General Concurrent PIC algorithm described in *Liewer and Decyk*[1989]. Extending the parallel electrostatic code to include the electromagnetic effects required no change in the parallel decomposition of the code. Run times for the studies in this paper range from four to fourteen hours.

In the code, variation is allowed in the x direction only, but all three velocity components must be calculated in order to calculate the $\mathbf{v} \times \mathbf{B}$ force on the particles and the transverse fields. At each time step, the new position of the $i-th$ particle is computed from

$$\frac{dx_i}{dt} = v_{x,i}$$

$$\frac{d\mathbf{v}_i}{dt} = \frac{q_i}{m_i}\Big(\mathbf{E} + \frac{\mathbf{v}_i \times \mathbf{B}}{c}\Big).$$

To update the fields at each time step, the plasma current density $\mathbf{j}(x,t)$ and charge density $\rho_q(x,t)$ are found at the grid points by interpolation from the particle positions. Only the transverse (y and z) components of the plasma current are needed. The longitudinal (along x) electric field is found by solving Poisson's equation, $\nabla \cdot \mathbf{E} = 4\pi\rho_q(x,t)$. The transverse (to x) electromagnetic fields, E_y,E_z, B_y, and B_z, are found by solving in Fourier space

$$\frac{\partial \mathbf{B}}{\partial t} = -\frac{1}{c}\nabla \times \mathbf{E}$$

$$\frac{\partial \mathbf{E}}{\partial t} = c\nabla \times \mathbf{B} - 4\pi\mathbf{j}.$$

In order to propagate the shock wave in a code using Fourier transform methods for the field solution, a simulation box with half plasma region and half vacuum damping region was used as described in *Lembége and Dawson* [1987b] to simulate an outgoing wave boundary condition in a periodic code. For this work the vacuum damping function was $f(i) = 1 - .25sin^2[\pi(x_i - L_x)/L_x]$ for $x_i > L_x$ and $f(i) = 1.0$ for $x_i < L_x$ where L_x is the length of the plasma region and $2L_x$ is the total system length. The shock was generated by driving a magnetic piston into the plasma by applying a large external current at several

grid points in the vacuum region also as described in *Lembége and Dawson* [1987b], where the external current was

$$j_{ext}(t) = \begin{cases} \frac{1}{2} j_0 \left[1 - cos(2\pi t/\tau)\right] & t < \tau/2; \\ j_0 & t > \tau/2, \end{cases}$$

where $\tau = 60\ \omega_{pe}^{-1}$ and where j_0 was in the range 100-400. (Here $\omega_{pe,i} = \sqrt{4\pi n e^2/m_{e,i}}$.)

An ion to electron mass ratio of $m_i/m_e = 1600$ was used for the runs presented in the paper. Many other runs were made with $m_i/m_e = 400$ to understand the scaling of the phenomena. The shocks angle $\theta_{\mathbf{Bn}}$ was varied from 90° to 60° by changing the direction of the upstream magnetic field from purely in the $\hat{\mathbf{z}}$ direction to a combination of $\hat{\mathbf{z}}$ and $\hat{\mathbf{x}}$. The length of the plasma region of the simulation box ranged from 1024 to 2048 c/ω_{pe}. Values of the parameter ω_{pe}/ω_{ce} ranged from 1 to 4 and values of β_e ranged from $10^{-3} - 10^{-1}$; results were quite sensitive to variations in these parameters. The ion to electron temperature ratio was in the range $T_i/T_e = 0.25 - 4.0$; the results were insensitive to variations in this ratio. A particle density of 20 particles per cell was used.

3. Simulation Results

3.1 Electron Heating by Trapping in Whistler Precursor

Figure 2 shows results at two times in a simulation for a shock with $M_A \approx 2.8$ (determined from the observed propagation speed), $\beta_e = 0.02$, $\omega_{pe}/\omega_{ce} = 2$, $m_i/m_e = 1600$, $T_i/T_e = 4$, and $\theta_{\mathbf{Bn}} = 70°$ (Case 1). Figures 2a-2d show $B_z(x)$, electron v_x and v_z phase space, and $\phi(x)$ respectively at $t\omega_{pe} = 600$ and Figures 2e-2f the same at $t\omega_{pe} = 1560$. Several features of the precursor wave train formation and electron-precursor interaction in low Mach number oblique quasi-perpendicular shocks are illustrated in this series of plots.

The plot of B_z at the later time (Figure 2e) shows a large well-developed whistler precursor wave train extending well ahead of the shock (Here, and in all the plots, $B_z(x)$ is normalized to $\sqrt{4\pi n_0 m_e c^2}$). The whistler precursor wave train results from the form of the dispersion relation for obliquely propagating magnetosonic waves, which, for a cold plasma, can be approximately written as

$$\omega^2 \simeq k^2 V_A^2 \left(1 + \frac{c^2 k^2}{\omega_{pi}^2} cos\theta_{\mathbf{Bn}}\right), \tag{1}$$

where $V_A = B/\sqrt{4\pi n m_i}$ is the Alfvén speed. From (1), it can be seen that the phase velocity of the whistlers is the Alfvèn speed for low k and increases with increasing k. Since the shock propagates at M_A times the Alfvèn speed, there is a wavenumber k_0 for which the phase velocity is the same as the shock velocity (see *e.g., Tidman and Krall*, 1971; *Mellott*, 1985), given by

$$k_0 \simeq \frac{\omega_{pi}}{c} \frac{\sqrt{M_A^2 - 1}}{cos\theta_{\mathbf{Bn}}}. \tag{2}$$

Theoretically, this whistler, which is stationary with respect to the shock, forms the standing precursor.

The wave number of the precursor at the shock front in Figure 2e is approximately that given by (1). For this run, (1) predicts $k_0 \simeq 7.6c/\omega_{pi}$ compared to an observed value of $k_0 \simeq 6.8c/\omega_{pi}$. Both the magnitude and the scaling of wave numbers of observed precursors in simulations with various Mach numbers, ion masses, and propagation angles are in basic agreement with (1). Plots of the y and z components of the magnetic field have verified that the precursor is elliptically polarized as expected for an obliquely propagating whistler wave.

The plots of B_z at the two times in Figures 2a and 2e illustrate the evolution of the whistler precursor wave train. The shock front acts as an "antenna" radiating whistler waves. The phase front of the wave train propagates faster than the shock, consistent with the observation of an increase in wave number in the packet with distance from the shock front. Throughout this run, the wavetrain continued to extend farther from the shock, with new wave crests appearing, until the run was terminated when the system boundary was reached. Although the precursor wave train did not reach a "steady-state" shape in this run, the amplitudes of the wavecrests nearer the shock front have reached steady-state amplitudes by the later time ($t\omega_{pe} = 1560$).

The decrease in amplitude of the precursors with distance from the shock front indicated the presence of some convective damping mechanism. From the electron v_x versus x phase space plots in Figures 2c and 2g, it can be seen that the electron are interacting strongly with the precursor wave train, suggesting that electron damping. Since v_x phase space is dominated by the electron motion parallel to the field for this $\theta_{\mathbf{Bn}} = 70°$ case, the electrons are apparently interacting with the precursor via the parallel electric field of the precursor. Because the shock is propagating at an angle $\theta_{\mathbf{Bn}}$ to the upstream magnetic field, there is a component of the shock and precursor electric fields parallel to the field:

$$E_{\|} = \nabla_{\|}\phi = cos\theta_{\mathbf{Bn}}\frac{d\phi}{dx} \ .$$

Plotted in Figures 2d and 2h is the normalized potential $e\phi/T_e^0$ where an electron with temperature T_e^0 has a Debye length equal to the grid spacing, e.g., $\Delta x = \sqrt{T_e^0/4\pi ne^2}$. (The length of the plasma region in this simulation was 2048 Δx.) The electrons can be freely accelerated along the field line by the potential and, if large enough, become trapped in it. In the plots, a positive gradient in the potential corresponds to a positive acceleration of electrons. Likewise, "hills" in the potential plots correspond to potential wells for electrons; valleys are potential wells for ions. Acceleration by the parallel electric field of the precursor is evident in the v_x phase space plots in Figures 2c and 2g; some evidence of trapping in the potential is also visible.

To determine whether the potential is large enough to trapped the electrons, the observed value of the potential well in the simulations can be compared to that required for trapping. The condition for parallel trapping in a potential well $\Delta\phi$ for an electron of velocity $v_{\|}$ is

$$\frac{1}{2}m_e(v_{\|} - v_{\|}^{ph})^2 < e\Delta\phi \ . \qquad (3)$$

Particles with velocities in the region $v_{\|}^{ph} - \Delta v_{\|} < v_{\|} < v_{\|}^{ph} + \Delta v_{\|}$ will be trapped where the trapping width $\Delta v_{\|}$ is given by

$$\Delta v_{\|} \sim \sqrt{\frac{2e\Delta\phi}{m_e}} .$$

The phase velocity of the precursor parallel to the field is much higher than the velocity in the direction of propagation x, $v_{\|}^{ph} = v_x^{ph}/cos\theta_{\mathbf{Bn}}$. Using $v_x^{ph} = M_A V_A$ for the standing precursor, the expression for the parallel phase velocity becomes $v_{\|}^{ph}/v_{te} = M_A V_A/v_{te} cos\theta_{\mathbf{Bn}}$. For the run in Figure 2, the electron temperature was $T_e = 0.5T_e^0$, and and Alfvén speed relative to the initial electron thermal speed was $V_A/v_{te} = 0.25$, yielding $v_{\|}^{ph}/v_{te} \approx 2$. The electron potential well of the first precursor in Figure 2d (labeled with an arrow) is $e\phi/T_e^0 \simeq 18$, giving a trapping width $\Delta v_{\|}/v_{te} \simeq 12$. Thus, even though the phase velocity is twice the thermal speed, the potential of the precursor is large enough to trap the entire electron distribution. The electron potential well of the second smaller precursor in Figure 2d is is $e\phi/T_e^0 \simeq 6.5$, giving a trapping width $\Delta v_{\|}/v_{te} \simeq 7$, and thus here, as well, essentially the entire distribution function can be trapped.

In the v_z phase space plot in Figure 2c, a trapping vortex at the location of the electron potential well of the leading precursor is most evident, although the effects of trapping by the larger precursor can be seen as well. The vortices are centered (in v_z) roughly at the parallel phase velocity $[v_{\|}^{ph} = (M_A V_A/cos\theta_{\mathbf{Bn}}) \approx v_{te}^0]$, indicated by the arrow at the edge of the plot. In the all phase space plots, velocities are normalized to $v_{te}^0 = \sqrt{T_e^0/m_e}$. Plots of the parallel electron distribution function $f(v_{\|})$ at this time show a well defined high energy tail. At the later time, although trapping vortices are not particularly well defined in the v_z phase space (Figure 2g), the high energy tails pulled out by trapping in all the whistler precursors can be seen. This strong wave-particle interaction between the electrons and the and the whistler is the most likely explanation for the observed spatial damping of the precursors near the shock front. For this simulation, the damping appears to be dominated by nonlinear (trapping) effects. However, if the run could be carried out for a longer time on a larger system so that a region of lower amplitude whistler were reached, a linear (Landau) damping region might also be observed.

The v_x phase space in Figures 2b and 2f at both times time shows that the trapping and acceleration in the parallel direction has led to a "heating" of the distribution in the perpendicular direction as well. Figure 3 plots $T_{\perp,1}$, the electron temperature in the direction perpendicular to $\mathbf{B}$ and $\hat{\mathrm{y}}$, as a function of time for electrons in the left one-third of the simulation box (behind the shock front). Here $T_{\perp,1}$ is normalized to T_e^0. The downstream temperature has increased by a factor of 8.5 over the upstream value. Adiabatic heating alone (from conservation of magnetic moment across the shock) $T_{\perp} \propto B$), would have increased the temperature by a factor of approximately 1.4. Thus trapping of the electrons in the potential of the precursor whistler has led to a significant heating of the electrons.

At $t\omega_{pe} = 600$, a much finer scale wave in B_z and in ϕ (Figure 2h; indicated by an arrow) can be seen at the same spatial location as the trapping vortex of the leading precursor. A finer scale wave is often seen at the same location of well-defined trapping

vortices and is probably a higher frequency whistler generated by the trapped electrons. This finer scale secondary oscillation is more evident in videos of the shock. (Copies of the "video," which play on a Mac II are available from the authors.)

3.2 Temperature Dependence of Damping and Electron Heating

If electron interaction with the parallel electric field of the precursor whistler is the cause of the electron heating and precursor damping as suggested by the simulation in Figure 2 (Case 1), then results should depend on the ratio of the precursor parallel phase velocity relative to the electron thermal velocity,

$$\frac{v_{\|}^{ph}}{v_{te}} = \frac{M_A V_A}{cos\theta_{\mathbf{Bn}} v_{te}} = \frac{M_A}{cos\theta_{\mathbf{Bn}}} \sqrt{\frac{2}{\beta_e} \frac{m_e}{m_i}} \,. \tag{5}$$

As this ratio decreases, trapped electrons are accelerated less relative to the thermal speed of the distribution, and a corresponding decrease in the relative heating is expected. However, as the parallel phase velocity falls further inside the distribution, more electrons interact with the wave and more damping is expected. Both of these effects are observed in the simulations when cases with three decreasing values of the ratio $v_{\|}^{ph}/v_{te}$ are compared.

Figures 2 and 4 show results for the magnetic field and electron v_x and v_z phase space from three simulations with varying values of electron temperature, with other parameters the same as in Case 1 (Figure 2). The plots are for the same time as the later plot in Figure 2, $t\omega_{pe} = 1560$. In the plots, all velocities are normalized to v_{te}^0, as in Figure 2. Case 2 (Figures 4a-4c) had a temperature higher by a factor of 4 ($v_{te} = v_{te}^0$); Case 3 (Figures 4d-4f) had a temperature higher by a factor of 16 ($v_{te} = 2v_{te}^0$). It can be seen that the upstream distribution function is wider in the warmer cases. The Mach number was insensitive to temperature, with $M_A \simeq 2.8$ for all three runs. The parallel phase velocity of the precursor was also relatively constant at $v_{\|}^{ph} \simeq v_{te}^0$. Thus for Case 2, $v_{\|}^{ph}/v_{te} \simeq 1$ and for Case 3, $v_{\|}^{ph}/v_{te} \simeq 0.5$, compared to $v_{\|}^{ph}/v_{te} \simeq 2$ for Case 1. The parameters for all cases shown in the figures are summarized in Table I.

Comparison of the precursor in the magnetic fields in Figures 2 and 4 (Cases 1-3) shows that the decrease in $v_{\|}^{ph}/v_{te}$, (from the increase in T_e), has lead to an increased convective damping of the whistler precursor. As the parallel phase velocity of the whistler falls further into the distribution function, more electrons interact with the wave, increasing the damping. Although the size of the precursor closest to the shock in the three cases is relatively unchanged, the spatial damping length decreases as the ratio $v_{\|}^{ph}/v_{te}$ decreases. This supports the interpretation that the convective damping is due to the interaction between the electrons and the parallel electric field of the precursor. For the warmest case, Case 3 ($v_{\|}^{ph}/v_{te} = 0.5$) where electron Landau damping should be strongest, the precursor wave packet has, in fact, reach a steady state, that is, the plot of the magnetic field for this run at a later time ($t\omega_{pe} = 1800$) showed no new wave crests and no further spatial extension of the wave train, but rather just a translation of the wave packet as seen in Figure 4d.

Comparison of Figures 2 and 4 also shows that the wavelength of the precursor closest to the shock has remained relatively unchanged, but that the wavelengths of the precursor more distant from the shock front is different in the three cases. The dominant wavelength of the precursor of the colder cases (Cases 1 and 2) decreases with distance from the shock front, whereas it is relatively constant in the warmest case, Case 3. This is probably due to the fact that the precursor wave train has not yet reached its steady state shape in Cases 1 and 2, whereas it has in Case 3. Presumably, if these cases could be continued, these shorter wavelength components to the precursor would propagate on ahead since their phase velocity is faster than the shock velocity. These shorter wavelength precursors are subject to more damping in the warmer case. Comparison of the potential plots in Figures 2 and 4 shows that the absolute size of the electron potential well of the first whistler is insensitive to temperature, with $e\Delta\phi/T_e^0 \simeq 15-18$ being a typical value for the well depth throughout the runs. However, comparison of the v_x phase space plots shows its effect on the electrons is quite different. For reference, the phase velocity of the precursor $v_{\|}^{ph} \simeq v_{te}^0$ is indicated with an arrow on the plots as in Figure 2. The v_x phase space in Figure 4c (Case 2) shows definite effects from the precursor, with a significant number of electrons pulled out of the distribution to form high a high energy tail, although less than in Figure 2c. The v_x phase space in Figure 4f (Case 3) shows much less effect from the precursor, with only a handful of high energy tail electrons evident. For Case 2 with $v_{\|}^{ph}/v_{te} = 1$ and $v_{te} \simeq v_{te}^0$, the trapping width relative to its thermal velocity is $\Delta v_{\|}/v_{te} \simeq 5-6$, and thus particles can be accelerated to velocities outside the initial distribution. For Case 3 with $v_{\|}^{ph}/v_{te} \simeq 0.5$, the trapping width is $\Delta v_{\|} \simeq 2.5 - 3v_{te}$, and thus less energetic tail formation is expected.

These differences are also evident in the v_x phase spaces. For Case 1, the region of v_x phase space behind the shock front in Figure 2b shows that the acceleration and trapping in the precursor has led to a "heating" of the electron distribution. For Case 2, the v_x phase space (Figure 4b) also shows some effect of heating, although considerably less than in Figure 2b. The v_x phase space in Figure 4e (Case 3) shows even less heating. For Case 2, the increase in temperature perpendicular to $\mathbf{B}$ and $\hat{\mathrm{y}}$, $T_{\perp,1}$, determined from the electrons in the left one-third of the box behind the shock front was $T_{\perp,1}^d/T_{\perp,1}^u \simeq 3.5$, where $T_{\perp,1}^d(T_{\perp,1}^u)$ is the downstream (upstream) temperature, compared to the increase of $T_{\perp,1}^d/T_{\perp,1}^u \simeq 8.5$ for Case 1. For the warmest case, Case 3, the temperature increase was $T_{\perp,1}^d/T_{\perp,1}^u \simeq 1.7$. (If the heating was adiabatic with $T_\perp \propto B$, the expected increase is $T_{\perp,1}^d/T_{\perp,1}^u \simeq B_\perp^d/B_\perp^u \simeq 2.3$). These results are summarized in Table I.

From these simulation results, we find that the important parameter in determining electron dynamics in weak quasi-perpendicular shocks is the ratio $v_{\|}^{ph}/v_{te}$. For $v_{\|}^{ph}/v_{te} < 1$, the phase velocity lies well within the distribution and the electrons damp the precursor more than when $v_{\|}^{ph}/v_{te} > 1$. For $v_{\|}^{ph}/v_{te} > 1$, the precursor will lead to more heating of the electrons as long as the a precursor potential is large enough to trap a significant portion of the distribution function. The amount of heating of the electrons by the precursor will increase as the value of the ratio increases above 1 and electron are accelerated to higher velocities relative to the initial thermal velocity.

Analysis of low Mach number oblique shocks from the earth's bow shock by *Mellott and Greenstadt*[1984](hereafter referred to as MG) suggested that electrons were important

in providing dissipation for low Mach number oblique shocks. The dissipation was evident only from the damping of the whistler precursor; the shocks widths themselves were consistent with laminar shock theory [Equation (2)]. Analysis of the same shocks by *Gary and Mellott*[1985] (hereafter referred to as GM) suggested linear electron Landau damping was an important dissipation processes for precursor whistlers; order of magnitude agreement was found between observed damping lengths and damping lengths predicted theoretically from linear electron damping. For parameters of the shocks analyzed in GM, the electron linear damping computed resulted from a resonance between the parallel phase velocity of the whistler and the electron motion along the field (Landau damping), not from cyclotron resonance and damping.

Although the simulation results in Figures 2-4 are for somewhat different values of β_e and M_A, the values of the parameter $v_{\|}^{ph}/v_{te}$ are similar and these simulation results support the conclusion of MG and GM regarding the importance of electron precursor damping with the addition caveat that nonlinear trapping and damping may also be present. The parameters of the shocks analyzed MG and GM were $\beta \approx 0.20$, $M_A \approx 2.0 - 2.3$, and $\theta_{\mathbf{Bn}} \approx 60 - 75°$. Using (5), this yields a range of values of $v_{\|}^{ph}/v_{te} \approx 0.3 - 0.7$.

We have seen no evidence on any parametric whistler wave decay processes; however, since the simulations were one-dimensional, any decay processes which would produce waves at an angle to the original wave are not allowed. Parametric decay processes might not show here because the daughter waves might be swept back into the shock by the flow. This is an area which needs more detailed study (experimental, numerical and theoretical).

3.4 Results for Lower Mach Number and for Larger $\theta_{\mathbf{Bn}}$

Figure 5 shows $B_z(x)$ for 4 times in a simulation with a lower Mach number, $M_A \approx 2.2$, within the range of the values for the same ISEE 1 and 2 shocks analyzed MG and GM. Other parameters for this case (Case 4) are the same as Case 1 ($\omega_{pe}/\omega_{ce} = 2.0$, $v_{te}/v_{te}^0 = 0.5$, $T_i/T_e = 0.25$, $\beta_e = 0.02$), but here the external current j_0 was lowered to reduce the shock Mach number. For this run, $v_{\|}^{ph}/v_{te} \approx 0.4$, which is in the range of the shocks analyzed by MG. Heavy damping of the precursor is observed here, as in Figure 4c, as expected for the value of $v_{\|}^{ph}/v_{te}$. The electron heating was also very small ($\sim 10\%$ increase in $T_{\perp,1}$ behind the shock at the late times).

In Figure 5, it can be seen that the precursor wave train evolves noticeably between $t\omega_{pe} = 1080$ and $t\omega_{pe} = 1320$. However, during the later interval ($t\omega_{pe}$ =1560 to 1800), there is little change in the shape of the precursor wave train. Thus here, as in Case 3, the heavy damping and shorter decay length of the precursor has allowed it to reach a "steady state" before the system boundary is reached.

Figure 6 shows $B_z(x)$ and v_z phase space at two times ($t\omega_{pe} = 240$ and 1200) for a simulation with a larger oblique angle, $\theta_{\mathbf{Bn}} = 60°$, and $M_A \simeq 3.0$(Case 5). Other parameters are the same as Case 1($\beta_e = 0.02, T_i/T_e = 4, \omega_{pe}/\omega_{ce} = 2$). Here $v_{\|}^{ph}/v_{te} \approx 1.5$, intermediate between Cases 2 and 3. For this case, damping is reduced so that, as in the other cases with $v_{\|}^{ph}/v_{te} > 1$, the precursor wave train has not reached a steady shape before it reaches the system boundary. The v_z phase space plot shows high energy tails and trapping vortices as expected for this case where $v_{\|}^{ph}$ lies above the thermal velocity

of the distribution. At $t\omega_{pe} = 240$, a well defined trapping vortex can be seen centered roughly at $v_z \approx v_{\parallel}^{ph} \approx 0.77 v_{te}^0$, indicated by the arrow at the side. Significant heating has occur in this case, with $T_{\perp,1}^d / T_{\perp,1}^u \simeq 2.2$ at late times. These results are also summarized in Table I.

4. Discussion

The simulation presented here have shown that electron interact strongly with the whistler precursor to laminar oblique quasi-perpendicular shocks via the whistler's parallel electric field. The electrons damp the whistler and are heated in the process. The electron dynamics depend strongly on the parameter $v_{\parallel}^{ph}/v_{te}$. Precursor damping increases as the parameter $v_{\parallel}^{ph}/v_{te}$ is decreased and and more electrons interact with the wave. For $v_{\parallel}^{ph}/v_{te} < 1$, precursor damping is observed with little electron heating. Significant electron heating is observed when $v_{\parallel}^{ph}/v_{te} > 1$. Using (5), the condition for a significant amount of electron heating can be written as

$$\beta_e < 2 \frac{M_A^2}{cos\theta_{\mathbf{Bn}}} \frac{m_e}{m_i}.$$

Thus for $m_i/m_e = 1836$ and $cos\theta_{\mathbf{Bn}} \simeq 0.3$, $\beta_e < 0.01 M_A^2$ is required. Thus the 1-D numerical simulations indicated that heating by the precursor whistler will be important in planetary and interplanetary shocks under low β_e conditions.

Earlier studies by *Lembége and Dawson*[1987a, 1989] also showed parallel acceleration and subsequent heating of the electrons by oblique quasi-perpendicular shocks. The parameter regime studied in the present work is different from that of earlier studies by *Lembége and Dawson*[1987a, 1987b]. Firstly, use of the concurrent computer has allowed us to run with realistic mass ratios ($m_i/m_e = 1600$ versus $m_i/m_e = 100$ in the earlier work) and to run for longer times; thus what was interpreted as a double layer [*Lembége and Dawson*, 1989] is, in fact, the beginning of the formation of the whistler precursor wave train. Secondly, in the present work, the Mach number of the shocks was sufficiently low so that no ion reflection occured.

The simulation results presented here were one-dimensional and thus did not include two dimensional effects such as cross-field ($k \perp B$) streaming instabilities driven by the electron current (*see e.g., Winske et al.*[1985] and references therein), electron current or two-dimensional parameteric decay instabilities which are other sources of wave damping and dissipation. To include the effect of the cross-field streaming instabilities in a self-consistent manner shock requires a 2-d full particle code [*e.g., Forslund et al.* 1984]. An ad hoc treatment via an anomalous collision frequency requires a fluid electron treatment as in hybrid particle ion-fluid electron codes. If cross-field instabilities also damp the whistler precursor, the effect of the electrostatic potential on the electrons will be weakened.

Thomsen et al.[1985] studied the electron and ion heating across the same 10 ISEE shocks analyzed by *Mellott and Greenstadt*[1984]. Electron and ion heating, both greater than adiabatic, were observed, with more ion heating than electron. Using the parameters in Table I of *Thomsen et al.*[1985] in (5), we find that in all cases, the ratio $v_{\parallel}^{ph}/v_{te} < 1$.

indicating heating from precursor trapping is not expected to be large for these shocks. Possibly electron precursor damping contributed to observed electron heating ahead of the shock ramp which will then be further heated by adiabatic compression. The analysis of *Thomsen et al.*[1985] was inconclusive as to what caused the heating, although heating from cross field instabilities in the lower hybrid range of was judged the most likely cause. This was supported by studies of electron and ion heating by lower hybrid range instabilities by *Winske et al.*[1985].

Whether or not cross-field streaming instabilities are unstable in an oblique quasi-perpendicular shock or its precursor depends on the value of the electron drift velocity

$$v_\perp = \frac{ck_0}{4\pi ne}\frac{\delta B}{B} \tag{6}$$

where k_0 is given by (2) and $\delta B/B$ is the relative jump in B. The condition for the fast Buneman cross field electron streaming instability to be unstable is $v_\perp/v_{te} > 1$. Using (6), this condition becomes

$$\frac{\sqrt{M_A^2 - 1}}{cos\theta_{\mathbf{Bn}}}\frac{V_A}{v_{te}}\frac{\delta B}{B} > 1. \tag{7}$$

(However, whether or not an instability is important will also depend on the shock width relative to the e-folding length of the instability.) Note the similarity between this condition and (5). The narrow parameter regime for which the Buneman mode is stable and (6) is satisfied is given by

$$\sqrt{M_A^2 - 1}\frac{\delta B}{B} < M_A.$$

Other, slower growing instabilities such as the lower hybrid drift and modified two stream [*Davidson and Krall*, 1977], are unstable for lower values of $v_\perp/v_{te}$. Thus in general, in the parameter regime for which electron heating via trapping in the precursor is expected to be large, slow or possibly fast growing cross-field instabilities might also be present. However, even if conditions for trapping and the Buneman instability are both satisfied, it is not clear which or if either will dominate. They will compete with each other and will probably effect each other. Two dimensional full particle simulations with realistic mass ratios will be necessary to determine what the effect of cross field instabilities is on electron trapping in the precursor and what effect any preheating might have on the instabilities themselves. Such simulations are extremely computationally intensive. The simulation results presented in this paper were obtained on a parallel computer with roughly the speed of a Cray. The work has demonstrated the utility of parallel computers for large scale plasma particle simulation problems; the next generation of parallel computers should make two-dimensional particle simulation codes with realistic parameters practical.

We have seen from these calculations that electron trapping in the potential of the whistler precursor wave train to a shock can be an important dissipation mechanism and lead to electron heating and precursor damping. It is thus clear that details of electron dynamics are important for some shock structures, and thus simple fluid approximations are likely to miss important aspects of the physics. The calculations presented here have simply pointed up the richness of the physical phenomenon that can exist in plasma shocks. They cast light on only a small part of this and there are many questions left unanswered by these simple 1D electromagnetic calculations.

Acknowledgements. We would like to thank D. Winske, M. Thomsen, and C. Kennel for useful discussions. The help of the JPL hypercube team, especially J. Crichton, C. Goodhart, R. D. Ferraro and J. E. Patterson is gratefully acknowledged. Part of the research described in this paper was performed at the Jet Propulsion Laboratory, California Institute of Technology and was sponsored in part by Caltech President's Fund Grant No. PF-317 and in part by the NSF Rice-Caltech-LANL Center for Research in Parallel Computation. The UCLA research was supported by Caltech President's Fund Grant No. PF-317 and by NSF Contract ATM 89-22133.

References

Birdsall, C. K., and Langdon, A. B., Plasma Physics via Computer Simulation, (McGraw-Hill, New York, 1985).

Davidson, R. C., and N. A. Krall, Anomalous Transport in high temperature plasmas with application to solenoidal fusion systems, *Nuc. Fusion, 17*, 1313, 1977.

Forslund, D. W., K. B. Quest, J. U. Brackbill, and K. Lee, Collisionless dissipation in quasi-perpendicular shocks, *J. Geophys. Res., 89*, 2142, 1984.

Gary, S. P. and M. M. Mellott, Whistler damping at oblique propagation: laminar shock precursors, *J. Geophys. Res., 90*, 99, 1985.

Lembége, B, and J. M. Dawson, Formation of double layers within an oblique collisionless shock, *Phys. Rev. Lett, 62*, 2683, 1989.

Lembége, B, and J. M. Dawson, Plasma heating through a supercritical oblique collisionless shock, *Phys. Fluids, 30*, 1110, 1987a.

Lembége, B, and J. M. Dawson, Self-consistent study of a perpendicular collisionless and nonresistive shock, *Phys. Fluids, 30*, 1767, 1987b.

Liewer, P. C., and N. A. Krall, Self-consistent approach to anomalous resistivity applied to theta pinch experiments, *Phys. Fluids, 11*, 1953, 1973.

Liewer, P. C., Numerical studies of ion reflection in collisionless theta-pinch implosions using a hybrid Vlasov-fluid model, *Nuc. Fusion, 16*, 817, 1976.

Liewer, P. C., and V. K. Decyk, A general concurrent algorithm for plasma particle-in-cell simulation codes, *J. Comp. Physics, 85*, 302, 1989.

Mellott, M. M., and E. W. Greenstadt, The structure of oblique subcritical bow shocks: ISEE 1 and 2 observations, *J. Geophys. Res., 89*, 2151, 1984.

Mellott, M. M., Subcritical collisionless shock waves, in *Collisionless Shocks in the Heliosphere: Reviews of Current Research* (B. Tsurutani and R. G. Stone, eds., AGU, Washington D. C.), p. 131, 1985.

Leroy, M. M., D. Winske, C. C. Goodrich, C. S. Wu, and K. Papadopoulos, The Structure of Perpendicular Bow Shocks, *J. Geophys. Res., 87*, 5981, 1982.

Leroy, M. M., C. C. Goodrich, D. Winske, C. S. Wu, and K. Papadopoulos, Simulations of a Perpendicular Bow Shock, *Geophys. Res. Lett., 12*, 1269, 1981.

Thomsen, M. F., J. T. Gosling, and S. J. Bame, Ion and Electron Heating at Collisionless Shocks Near the Critical Mach Number, *J. Geophys. Res., 90*, 137, 1985.

Tidman, D. A., and N. A. Krall, *Shock Waves in Collisionless Plasmas*, p. 24, Wiley-Interscience, New York, 1971.

Winske, D. and M. M. Leroy, Hybrid Simulation Techniques Applied to the Earth's Bow Shock, *Computer Simulation of Space Plasmas*, Terra Scientific Publishing Company, 1981.

Winske, D., M. Tanaka, C. S. Wu, and K. B. Quest, Plasma Heating at Collisionless Shocks Due to the Kinetic Cross-Field Streaming Instability, *J. Geophys. Res.*, *90*, 123, 1985.

J. M. Dawson and V. K. Decyk, Physics Department, University of California, Los Angeles, CA 90024.

B. Lembège, CRPE/CNET, Issy-les-Moulineaux, France.

P. C. Liewer, Jet Propulsion Laboratory, California Institute of Technology, MS 198-136A, 4800 Oak Grove Drive, Pasadena, California 91109.

Table I. Summary of Cases and Results

Case	$\theta_{\mathbf{Bn}}$	v_{te}/v_{te}^0	M_A	$v_{\parallel}^{ph}/v_{te}$	$T_{\perp}^u/T_{\perp}^d$	$B_{\perp}^u/B_{\perp}^d$
1	70°	0.5	2.8	2.0	8.5	2.3
2	70°	1.0	2.8	1.0	3.5	2.3
3	70°	2.0	2.8	0.5	1.7	2.3
4	70°	0.5	2.2	0.4	1.1	1.8
5	60°	2.0	3.0	1.5	2.2	1.8

Figure Captions

Fig. 1. Low Mach number oblique terrestrial bow-shocks measured by the ISEE 1 spacecraft. Shown in the top panels are high-resolution, unfiltered total magnetic field profile data showing the whistler precursor wave-train. The lower panels show filtered data on an expanded time scale (from *Mellott and Greenstadt*[1984]).

Fig. 2. Simulation results at two times from Case 1 for B_z (normalized to $\sqrt{4\pi n_0 m_e c^2}$), electron v_x and v_z phase space, and the electrostatic potential ϕ (normalized to T_e^0/e, see text). The effect of the precursor wave train on the electrons can be seen in the phase space plots. For this case, $v_{\|}^{ph}/v_{te} \approx 2.0$. In 2d, the arrow shows the *electron* potential well of the first precursor. This precursor, as well as the smaller precursor, is large enough to trap the entire electron distribution. In 2h, the arrow shows a finer scale secondary wave which appears to be associated with the trapped electrons.

Fig. 3. Plot of the electron temperature in the direction perpendicular to $\mathbf{B}$ and $\hat{y}$, $T_{\perp,1}$ (normalized to T_e^0) in the left one-third of the simulation box as a function of time for Case 1. The perpendicular heating resulting from the precursor and shock has led to a factor of 8.5 increase in the temperature.

Fig. 4. [a-d] Simulation results for Case 2 for B_z, electron v_x and v_z phase space, and the electrostatic potential ϕ, all at the same time as the later pictures in Fig. 2 ($t\omega_{pe} = 1560$). Parameters are the same as Case 1 (Figure 2) except ($v_{\|}^{ph}/v_{te} \approx 1.0$). [e-g] Simulation results for Case 3 for the same parameters as Case 1 and 2 except $v_{\|}^{ph}/v_{te} \approx 0.4$. More convective damping of the precursor wave train is evident in the warmer case, Case 3. $M_A \approx 2.8$ for Cases 1-3.

Fig. 5. Magnetic field profilee B_z at 4 time increments from Case 4 for a lower M_A number shock ($M_A \approx 2.2$, $v_{\|}^{ph}/v_{te} \approx 0.4$). At the later times, the precursor wave train has reached a "steady-state" shape, *e.g.*, , the amplitude of the precursors do not change (nor do new wave crests appear) as the shock propagates. Electron interactive with the precursor potential has convectively damped the precursor to the noise level in about four wavelengths. $\theta_{\mathbf{Bn}} = 70°$ for Cases 1-4.

Fig. 6. Results for B_z and v_z phase space from Case 5 ($v_{\|}^{ph}/v_{te} \approx 1.5$, $\theta_{\mathbf{Bn}} = 60°$) at two times in the simulation. The precursor wave train is still evolving when the system boundary is reached. A trapping vortix is evident at the early time, centered in v_z at approximately the parallel phase velocity of the precursor, shown by the arrow at the side.

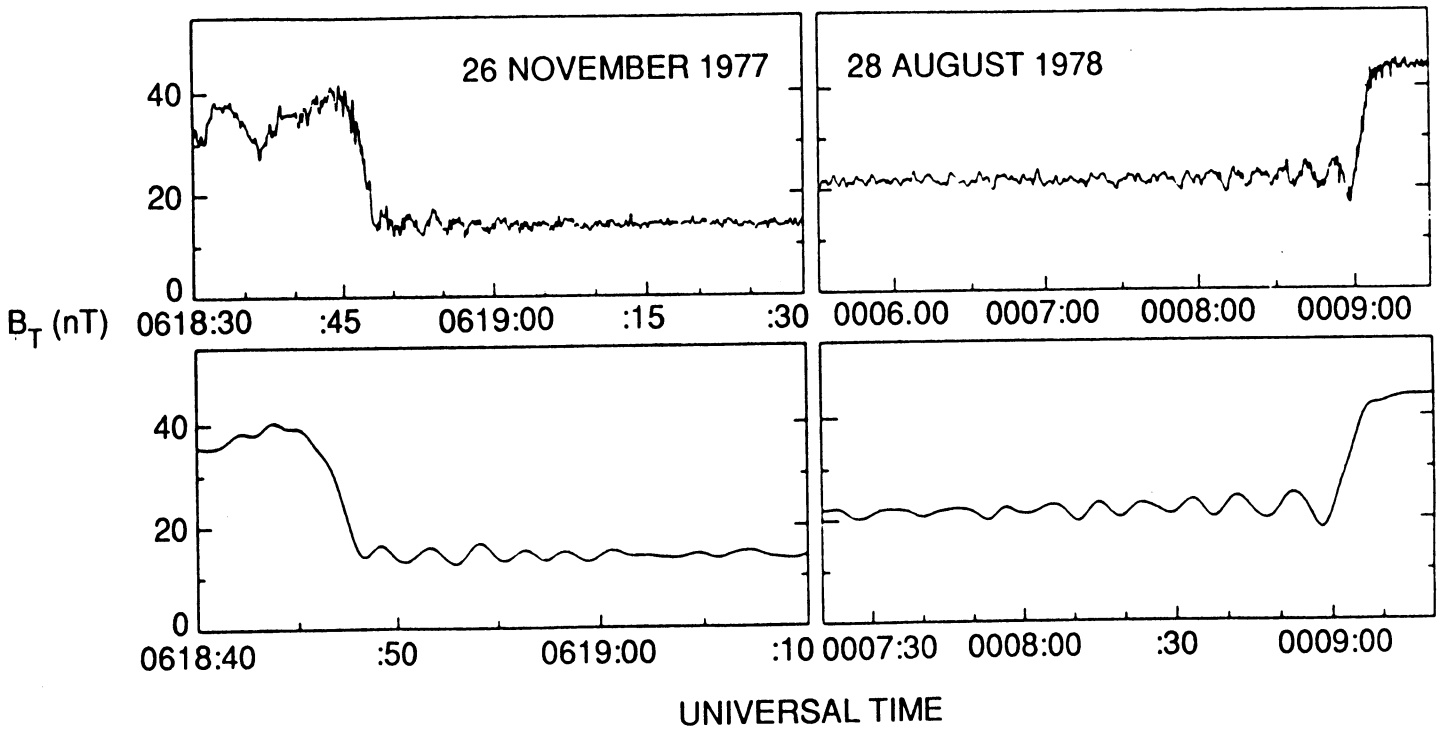
26 NOVEMBER 1977
28 AUGUST 1978
40
20
0
B_T (nT)
0618:30
:45
0619:00
:15
:30
0006.00
0007:00
0008:00
0009:00
40
20
0
0618:40
:50
0619:00
:10
0007:30
0008:00
:30
0009:00
UNIVERSAL TIME

Fig. 1

CASE 1

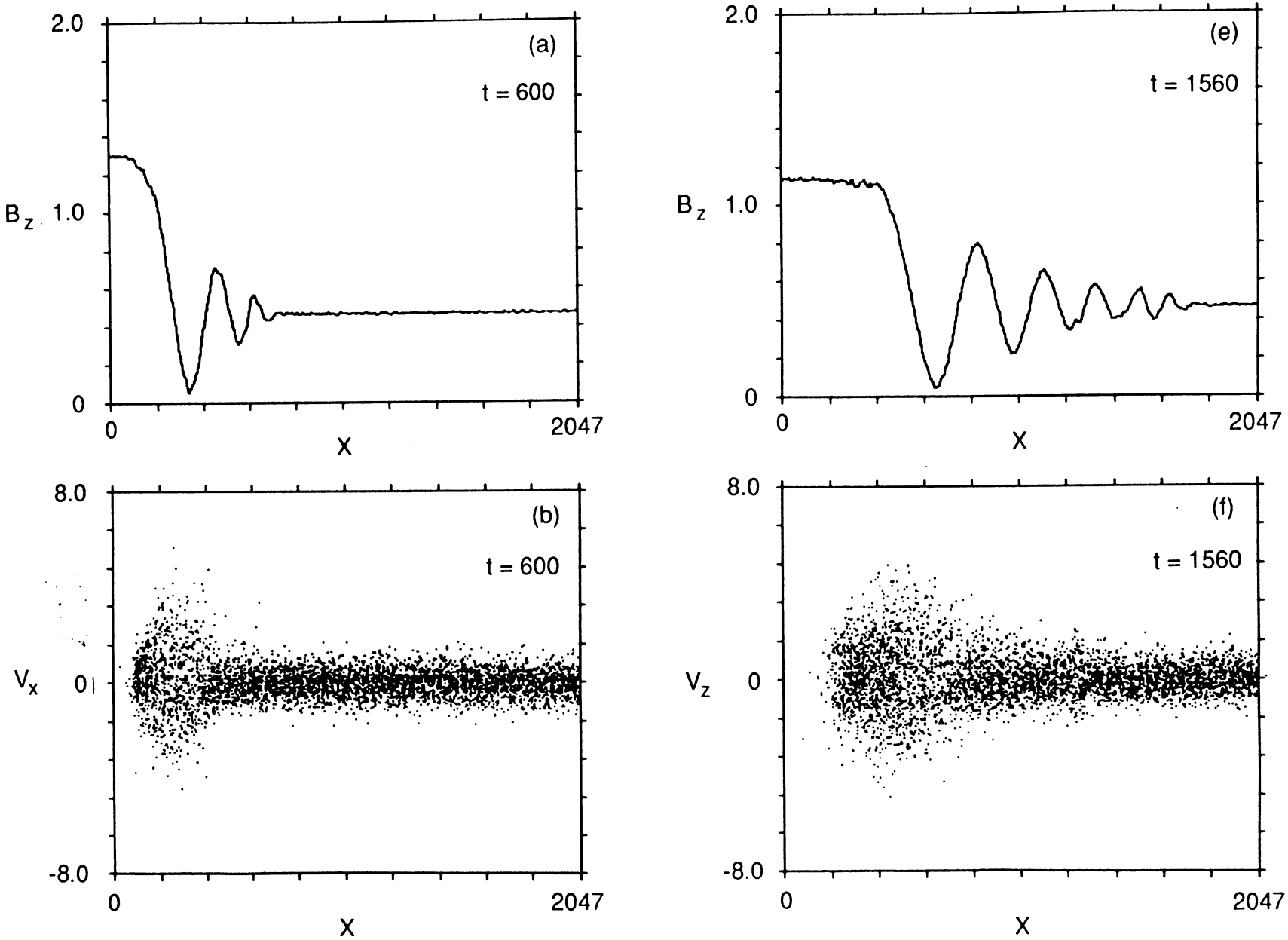
(a)
t = 600
2.0
1.0
0
B_z
0
2047
X
(e)
t = 1560
2.0
1.0
0
B_z
0
2047
X
(b)
t = 600
8.0
0
-8.0
V_x
0
2047
X
(f)
t = 1560
8.0
0
-8.0
V_z
0
2047
X

Fig. 2

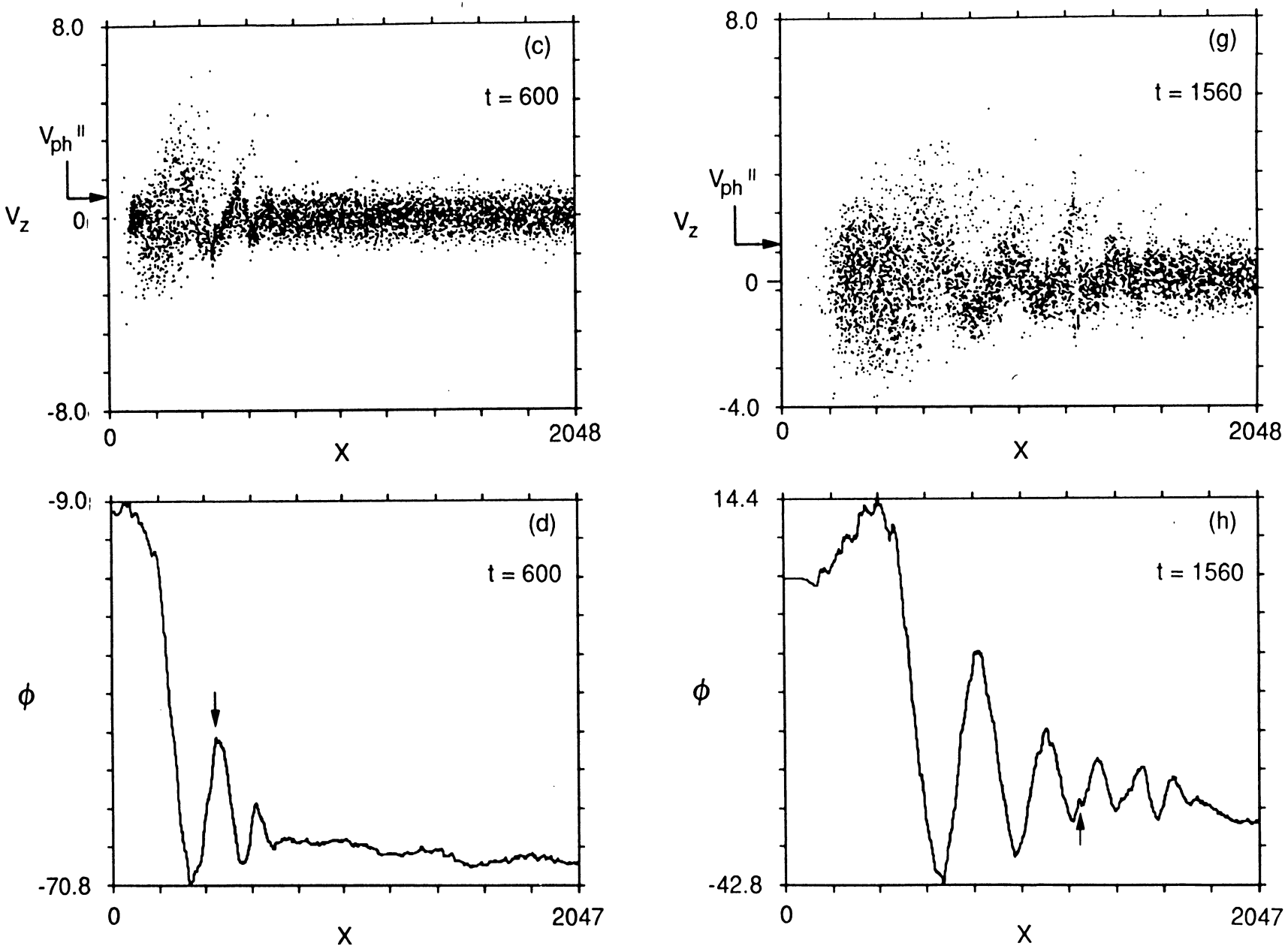
8.0
(c)
t = 600
$V_{ph}^{\parallel}$
V_z
0
-8.0
0
2048
X
8.0
(g)
t = 1560
$V_{ph}^{\parallel}$
V_z
0
-4.0
0
2048
X
-9.0
(d)
t = 600
ϕ
-70.8
0
2047
X
14.4
(h)
t = 1560
ϕ
-42.8
0
2047
X

Fig. 2 - cont.

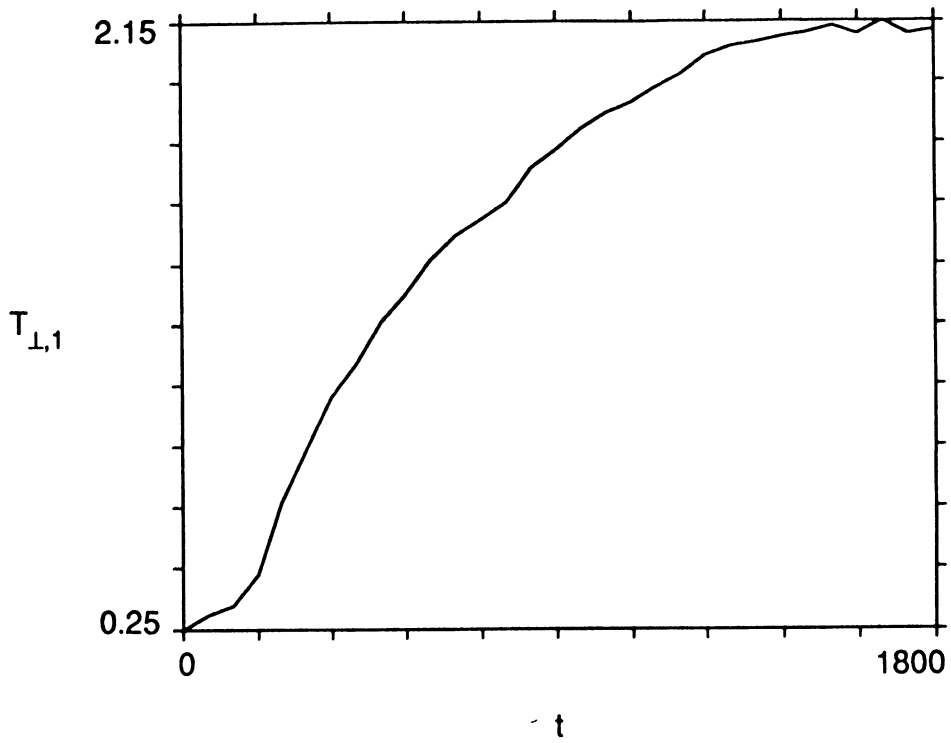

Fig. 3

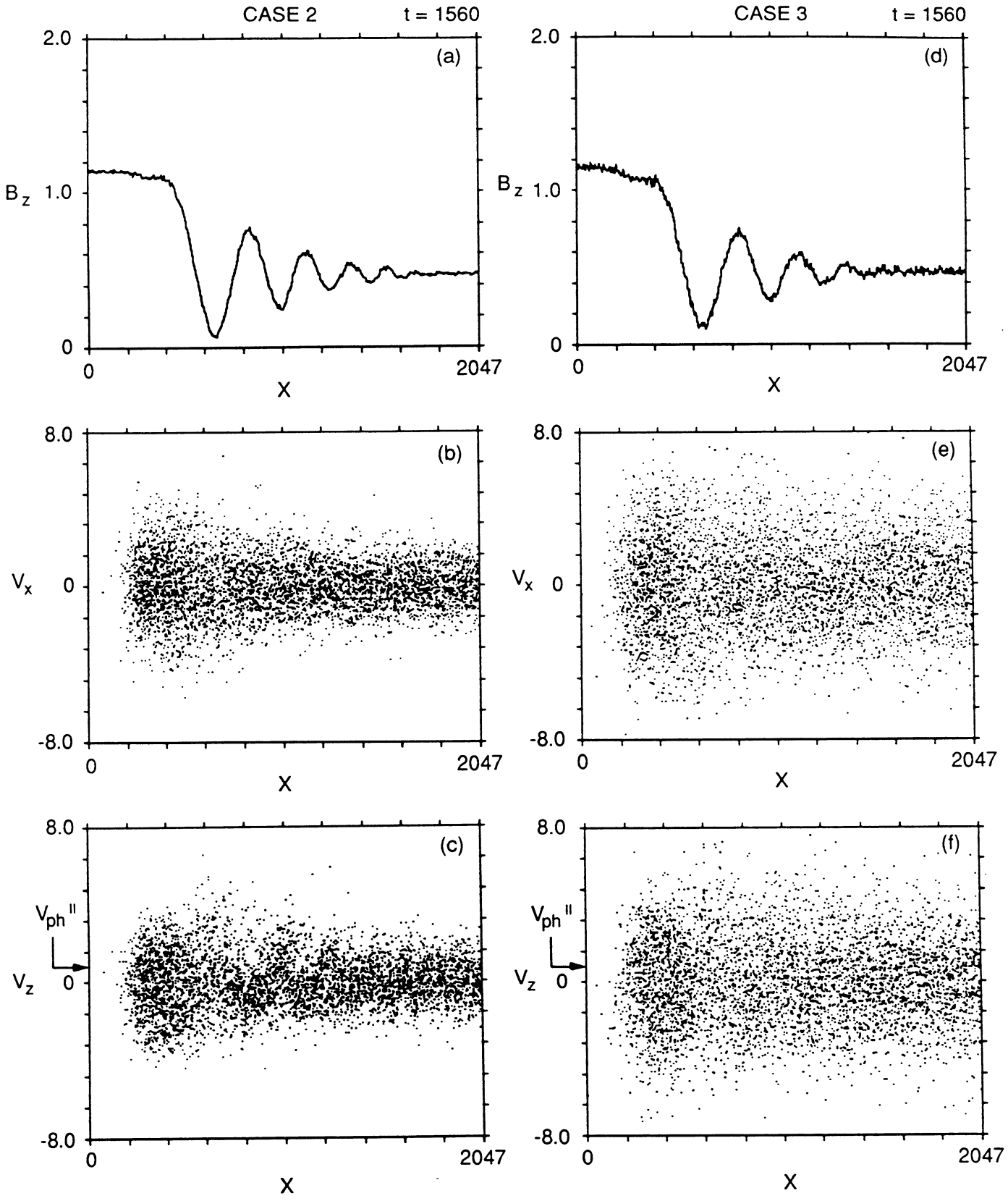
CASE 2
t = 1560
CASE 3
t = 1560
(a)
(b)
(c)
(d)
(e)
(f)
2.0
1.0
0
B_z
8.0
-8.0
V_x
V_z
$V_{ph}^{\parallel}$
0
2047
X

Fig. 4

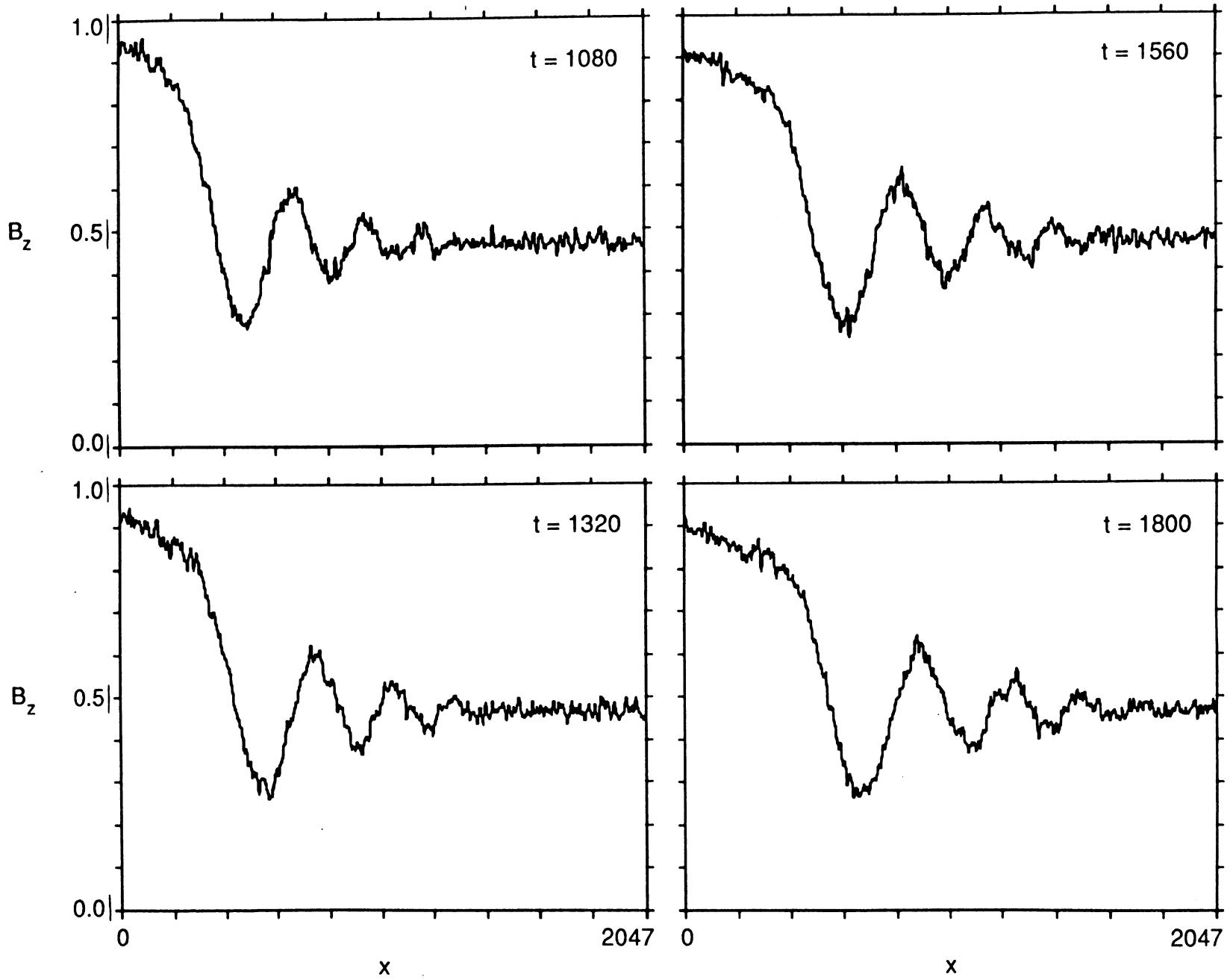

Fig. 5

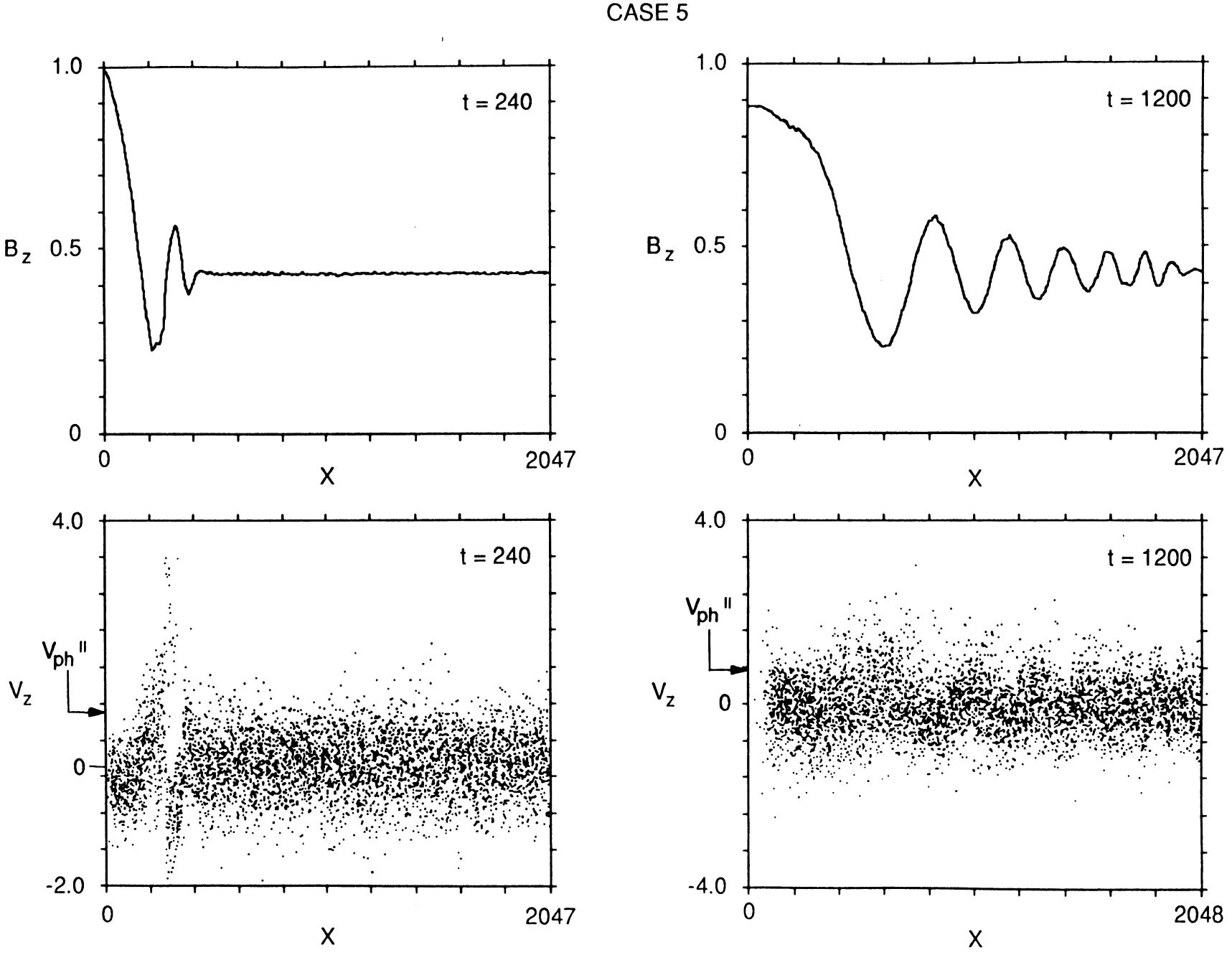
CASE 5
1.0
t = 240
B_z 0.5
0
0
X
2047
1.0
t = 1200
B_z 0.5
0
0
X
2047
4.0
t = 240
V_{ph} ||
V_z
0
-2.0
0
X
2047
4.0
t = 1200
V_{ph} ||
V_z
0
-4.0
0
X
2048

Fig. 6